FEATURED ARTICLE

ΔF_{signal}

The signal (ΔF_{signal}) is a deviation from the baseline fluorescent intentisy (F_b). The size of ΔF_{signal} varies depending on the sensitivity of the dye to neural activity in response to the same amount of change to the membrane potential. The ΔF_{signal} of most modern VSDs report a 10^{-3} to 10^{-2} change in the F_b in response to physiological neuronal activity from neural tissue. Both ΔF_{signal} and F_b are proportional to the light intensity applied to the specimen.

ΔF_{shot}

Photon shot noise is a noise source related to the light intensity; other sources of noise come from mechanical movement and the fluctuation of the light source. There are several ways to reduce the latter noise sources. However, there is no way to reduce photon shot noise (ΔF_{shot}) because it depends on the quantal nature of light. Photon shot noise is the fluctuation of the number of photons being detected by the detector, which is proportional to the square root of the total number of detected photons.

ΔF_{dark}

The dark noise (ΔF_{dark}) is a constant noise caused by the electrical measurement system. In the case of the CCD imager, the most conspicuous component of the ΔF_{dark} is the thermal noise of the photo-diode (KTC noise). Cooling the CCD imager can reduce this noise (so called "cooled CCD camera"). On the other hand, in the CMOS imager, current leakages at the FET switching gate have a much stronger contribution to the thermal noise.

Figure 1(A) shows these components as a function of the initial fluorescence (F). Plots of ΔF_{signal} with sensitivities of 10^0, 10^{-1}, 10^{-2}, and 10^{-3} are shown. ΔF_{shot} is shown by the thick line, and ΔF_{dark} is shown by the dashed lines, representing constant values in the figure. Signals with amplitudes below ΔF_{shot} and ΔF_{dark} will be obscured by those noises. Hence, ΔF_{signal} with higher sensitivity can be recorded at a lower light intensity where the ΔF_{dark} of the imager is sufficiently low. On the other hand, for most VSDs, dyes that can report 10^{-4} to 10^{-3} [14, 15] were not detectable at below 10^4 photons when CCD imagers were used. A photodiode array (PDA) or CMOS imager needs over 10^5 photons because of the high levels of dark noise.

Figure 1(B) shows the signal-to-noise ratios (SNRs) of signals with $\Delta F/F$ values of 5×10^{-3} and 2×10^{-3}, recorded with ΔF_{dark} levels of 200, 1000, and 5000 photons. A ΔF_{dark} value of 200 corresponds to the signal recorded with a CCD imager, 1000 photons corresponds to CMOS and PDA, and 5000 photons are for those imagers with worse dark noise levels. As is clear in the figure, the same signal gives a better SNR with lower ΔF_{dark} values especially at lower F. On the other hand, if the F is increased, the signal can give a better SNR since the SNR increases proportionally with the square root of F [16].

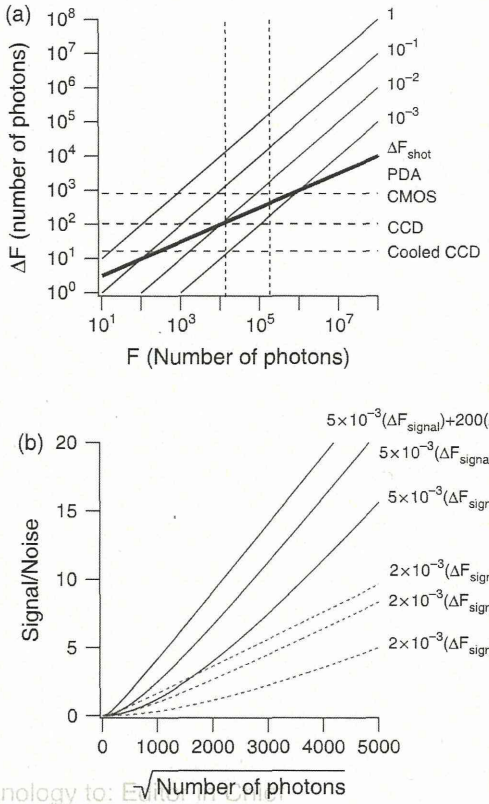

Fig. 1. (a) A schematic illustration showing the change in the light intensity (ΔF) as a function of basal light intensity (F). The lines labeled 1, 10^{-1}, 10^{-2}, and 10^{-3} show the optical signal generated by fluorescent reporters, showing the fractional changes of those amounts (that is, 1, 10^{-1}, 10^{-2}, and 10^{-3}) with respect to F. respectively (i.e., ΔF_{signal}). The thick line shows the amount of photon shot noise (ΔF_{shot}), which is proportional to the square root of F. The horizontal dashed lines shows the constant dark noise level (ΔF_{dark}) corresponding to a PDA/CMOS camera, a CCD camera, and a cooled CCD camera. The vertical dashed line represents a realistic F level suitable for VSD imaging with a 10^{-3} to 10^{-2} change. (b) Signal-to-noise ratios calculated for a 5×10^{-3} and 2×10^{-2} change of neuronal activities acquired with three different types of camera. A ΔF_{dark} value of 200 represents most CCD cameras, 1000 represents PDA/CMOS cameras, and 5000 represents those with worse dark noise.

A larger F is better for a high S/N, but it has a high probability of causing side effects to the subjects, like photo-induced toxicity, photo-bleaching, and, in some extreme cases, heating. To avoid this, it is important to have highly sensitive reporters and an imager with a lower noise level.

A FAST NEURONAL SIGNAL REQUIRES A HIGHER-BRIGHTNESS SIGNAL

The number of photons captured at a photodiode is dependent on the sampling rate of the system. The membrane

potential response of the neurons occurs within the millisecond range, e.g., an action potential occurs within a few milliseconds. In order to follow these changes, the sampling rate should be in the sub-millisecond range (0.1 ms to 0.5 ms). The extremely short accumulation time makes it difficult to accumulate many photons for measurements.

What is a "bright" fluorescent image under many other biological imaging schemes used for slower biological events, such as Ca^{2+} imaging, often becomes a "dark" image under optical imaging with VSD. Simply, imaging of a biological process that occurs on the scale of seconds is about 1000 times brighter than that occur on the scale of milliseconds such as fast membrane potential change.

EQUIPMENT NEEDED TO PERFORM VOLTAGE-SENSITIVE-DYE IMAGING

In this section, we discuss the requirements for equipment to perform VSD imaging.

Optics

Because the "brightness" of the image is primarily important for seeing the signal in spite of the effect of ΔF_{shot}, proper optics are important. The brightness at the detector is a function of

(1) the fluorescence excitation light intensity,
(2) the fluorescent emission (the product of the extinction coefficient and the fluorescent quantum yield) of the dye in the specimen,
(3) the efficacy of the optics in correcting the light, and
(4) the magnification of the optics.

Among these, the efficacy of the optics scales as the fourth power of the numerical aperture (NA) of the optics when epi-fluorescent illumination is applied. The light intensity at the detector scales as the inverse square of the magnification of the optics.

Because the size of the neural circuit is relatively large, relatively low-magnification optics are needed. However, most existing microscopes do not have a high enough NA at this low magnification, probably because the light intensity itself is already enough for the usual imaging at this low magnification. A high NA at low magnification with a large focus length (f) requires a large pupil. To fulfill this requirement, epifluorescence optics with high numerical aperture were built using a tandem-lens configuration [17, 18].

Imaging System

As we discussed above, VSD imaging is usually carried out under far brighter conditions than other biological imaging techniques. Hence, one of the key features of the detector system for VSD imaging is the photon-well depth of the detector, that is, how many photons can be detected at the detector.

Early attempts to acquire the optical signal involved using arrays of a relatively small number of photo-diodes, with arrays of increasing size over time including such grid sizes as 5×5, 10×10, 12×12, 16×16, 22×22, and 24×24 [5, 6, 19–21]. The photo-diode configurations have improved speed because of the parallel readout and deep photon-well depth ($>10^6$). On the other hand, the spatial resolution is naturally limited. In addition, the ΔF_{dark} is relatively large.

In order to perform high-resolution imaging, passive charge-coupled devices (CCDs) and active pixel sensors such as complementary metal–oxide–semiconductor (CMOS) image sensors have been used for VSD imaging [22, 23]. Those systems can acquire 30,000 pixels at 555 frames per second and 10,000 pixels at 10,000 frames per second, respectively.

Experimental Chamber System

Mechanical noise, i.e., movements of the subject under the field of view, easily reached over 100%. That is, if a bright object, such as the edge of a tissue, moved into a dark background, the fractional change at the pixel could easily exceed 100%. Such huge noises have to be avoided to measure signals with a sensitivity of 10^{-3}. In the case of *ex vivo* preparation such as slice preparation, most of the mechanical noises can be avoided by the proper use of an anti-vibration table, often used for electrophysiological experimental rigs. Often the fixation of the preparation in the experimental chamber causes the problem. We solved this problem by introducing a new chamber system, shown in Figure 2 [18]. In this system, the slice preparation is held in place, attached to the membrane filter, which is fixed to a plexiglass holding ring. The ring is held in the experimental chamber firmly so the sample does not move appreciably with respect to the chamber. Another advantage of the chamber is that the amount of expensive VSD needed to stain the slice can be kept to a minimum. In the case of the chamber shown in Figure 2, only 100 μl of the staining solution is needed to stain a slice.

Devices to Inhibit Vibration of the Surface of the Fluid

The other source of mechanical movements is caused by the flow of solution needed to keep the preparation alive. That flow produces small movements in the surface of the fluid in the experimental chamber. To minimize this effect, it is advantageous to use a water immersion objective lens. However, the range of available water immersion objective lenses of low magnification with high numerical aperture is limited. We requested custom objective lenses from Olympus (×5, NA 0.35, ×10 NA 0.60). Recently Brainvision

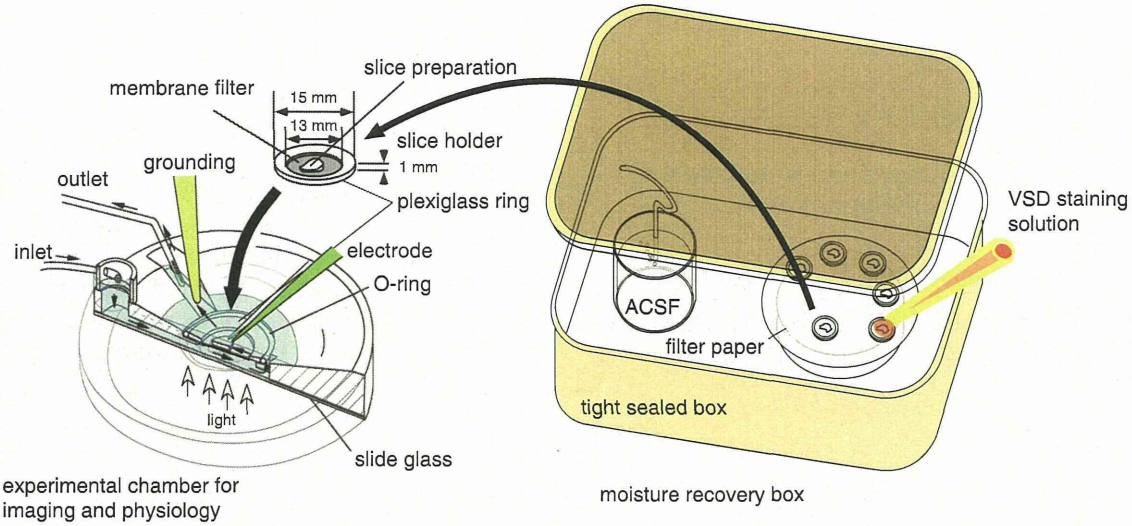

Fig. 2. An illustration of the experimental chamber system. The illustration on the left shows the experimental chamber, holding a slice preparation held on top of a membrane filter supported by the plexiglass ring (the slice holder ring). The physiological solution is fed to the chamber from an inlet and run under the membrane filter; then it flows over the slice and is sucked up by an outlet tube. An electrical ground was installed near the outlet port. The slice can be accessed by electrode and can be observed with transmitted light and epi-fluorescence. The slice holder rings, along with a slice, are placed on filter paper covering on a container filled with physiological solution, which is kept in the tight sealed box filled with moist air with CO_2/O_2 gas bubbled into the solution. When staining the slice, an aliquot of staining solution (100 μl) is applied to the slice holder, which should be washed out after the proper staining duration.

Inc. released a water immersion objective lens with similar specifications ($f = 20$ mm, NA 0.35).

If a wider field of view is needed to conduct experiments, the work-around is to put a small piece of slide glass of the surface of the fluid. We often use a small piece of glass (10 mm × 6 mm × 1 mm) attached to a holding bar, which is then attached to a small manipulator.

Illumination

Selection of illumination is also important. Brighter illumination such as that by mercury and xenon arc discharge lamps has not been suitable for VSD imaging because of the fluctuation of the arc. However, some recent xenon lamps have better stability and can be used for VSD imaging. The laser can also pose problems because of the speckle noise due to the high coherence. The most commonly used source for the illumination is a halogen light. It is not brighter, but it is stable and suitable for low magnification applications because of the wideness of the filament. The rapid progress in increasing the available power from LEDs indicates that LEDs are indeed useful for VSD imaging.. However, one must choose an LED illumination with temperature compensation because of the heat-induced drift [24].

Voltage-Sensitive Dye

Since the first attempt to produce voltage-sensitive probes [3, 4], continuous efforts have been made to produce better voltage-sensitive dyes [10, 11]. VSDs can be classified into two major categories based on the response time after a change to the membrane potential—slow dyes and fast dyes—depending on the mechanisms by which they change the optical signal in response to a change in the membrane potential [12]. The slow dye responds to a change in the membrane potential due to the change in distribution (partitioning) of the dye across the membrane. Those slow dyes have not often been used to monitor neuronal signals. The fast dye uses a different mechanism, and it can attain a reaction time below the order of a microsecond [25, 26]. For following neuronal activity, the fast dye is suitable. A practical measure of the differences in VSDs that is often used is their solubility in saline solution. The VSDs that are rather easily soluble in water are RH-795, RH-482 [10], Di-2-ANEPPQ (JPW1114) [27], and RH-1692 (blue dye) [28]. Those VSDs are easily soluble in saline and rather easy to use. The major drawback of those kinds of VSDs is that they can easily be washed out by perfusion with aqueous solution. These characteristics made those dyes difficult to use in *in vitro* preparations, but rather favorable in *in vivo* preparations [1, 11] and isolated brain preparations [2, 29]. In contrast, VSDs that are rather difficult to dissolve in saline, lipophilic dyes, are rather difficult to use but are resistant to wash-out; examples include Di-4-ANEPPS and Di-8-ANEPPS [3, 4, 26]. For brain slice preparation, we prefer the lipophilic styryl dye Di-4-ANEPPS that uses electrochromism to show the fluorescence changes upon membrane potential changes [5–7, 12]. The dye showed a better S/N ratio and was stable over very long experiments [8–10, 14, 18, 30]. Di-4-ANEPPS can be used with

isolated whole brain preparation when applied from the outside of the tissue [11–13, 31].

OPTICAL SIGNAL IN *EX VIVO* SPECIMEN

In the following sections, we will see several applications of optical recordings to *ex vivo* specimens.

Optical Signal in Hippocampal Slice Preparation

Because of its simple lamellar organization [14, 15,32, 33], the *in vitro* hippocampal slice (Fig. 3(b)) preparation is ideal for studying neural integration in neural circuits with VSD imaging from the earlier attempt to apply the VSD imaging to mammalian brain tissue [16, 34]. This was extended to show pharmacological study of synaptic connections with an absorption dye [17, 18, 35–38] and later with a fluorescent dye [5, 6, 14, 18–21, 39–47]. The control of the synaptic plasticity [22, 23, 30, 48–52] and dendritic functions [18, 53–56] have also been examined with the VSD imaging method. This allows direct viewing of the hippocampal layers, thus allowing the optical signals to be attributed to specific membrane areas of the major cell type, the pyramidal cell. For example, neural integration in

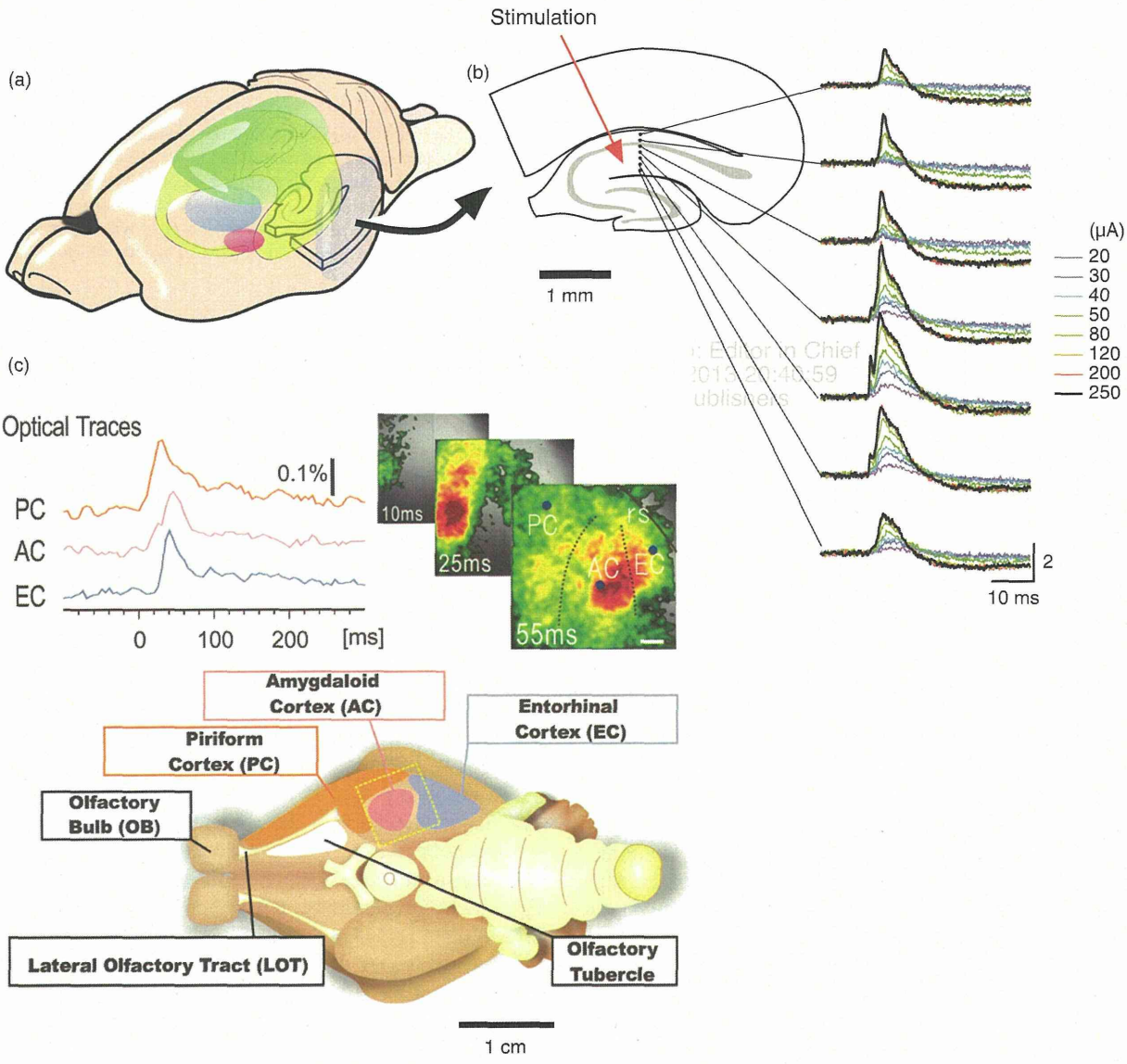

Fig. 3. An illustration of the whole brain of a rat (a) and a slice (b) with optical signal traces at various stimulus intensities of 20, 30, 40, 50, 80, 120, 200, and 250 μA respectively applied to the Schaffer collaterals of area CA1. (c) Representative optical traces under electrical stimulation of the lateral olfactory tract (LOT) appeared in the piriform cortex (PC), amygdaloid cortex (AC), and the entorhinal cortex (EC) of the isolated whole brain preparation of the guinea pig. The spread of activity in the field of view shown by the dotted line on the bottom illustration of the isolated whole brain was also shown in the upper right side of (c).

area CA1 can be assessed by examining signals in stratum radiatum, which correspond primarily to the membrane potential responses of pyramidal cell apical dendrites, and signals in stratum pyramidale, which correspond primarily to membrane potential responses of pyramidal cell somas.

The nature of the optical signals was that of a population signal. For example, even if the stimulus intensity is high enough to obtain saturated population spikes, the optical signals measured from stratum radiatum (which correspond to a few tens of millivolts of excitatory postsynaptic potential [EPSP]), are larger than those measured from stratum pyramidale (which correspond to over a hundred millivolts of action potential). The disparity could be caused by a differential VSD sensitivity to different parts of the membrane and/or by the nature of the population signal. We confirmed that a ten-fold increase of the external potassium concentration of saline caused uniform depolarizing of the VSD optical signal. This finding supports the idea that the disparity of the amplitude distribution of VSD is caused by the nature of the population signal. In addition our NEURON simulation showed that the amplitude distribution of the VSD signal can be explained by the population nature of the signal [24, 46].

Optical Signal of Other Slice Preparations

The optical recording methods can also be useful for visualizing the neural activities of other types of slice preparations. Tanifuji et al. showed horizontal propagation in rat visual cortical slices [3, 4, 57]. Yuste et al. analyzed a rat cortical neural network with Di-4-ANEPPS. The recent application of VSD to the thalamo-cortical connection [10, 11, 58], and the connection between the entorhinal cortex and other cortices [12, 59–61] and the connection between the entorhinal and hippocampal structures [25, 26, 62], and the amlygdala and perirhinal-entorhinal cortex [10, 63] shows the usefulness of applying VSD to larger interactions among regions of the brain circuit.

Optical Signal in Isolated Brain and CNS Preparation

The other types of *ex vivo* specimens used for optical recordings are isolated whole brain preparations [27, 31, 64] from guinea pigs. By applying the optical imaging technique to this preparation, we can monitor the spread of neural activity across limbic cortices such as the amygdaloid and entorhinal cortices, which is a difficult process to expose under *in vivo* conditions. The effective and efficient monitoring of the fractional changes of fluorescence from such large cortical areas requires the combined use of a macroscopic microscope and a camera with a large imager (e.g., $\geq$2/3 inch CCD).

In addition to such advantages of a widespread intact synaptic network, isolated brain preparation has excellent mechanical stability, where the stability is affected most often by circulatory and respiratory activity under *in vivo* conditions. Thus, in various studies, similar approaches have been used.

Isolated brain stem preparations have been used for the study of respiratory neural circuits [28, 65–67]. Purkinje cell function has been studied with isolated *in vitro* cerebellum preparation from neonatal rats [68, 69]. Another interesting use of *ex vivo* preparation is to investigate membrane potential events during the developmental process of chick brain stem preparation [70, 71].

CONCLUSION AND PERSPECTIVE

Single-photon wide-field voltage-sensitive-dye imaging has now been developing for more than two decades and steadily acquiring a wider range of users. These methods are still useful for visualizing the neural circuit activities over a wider range in the brain. The changes in wider neural connection often are important for distinguishing healthy and pathological conditions in most disease recognition processes [72]. We recently developed new confocal optics that can be used for these applications [73].

For these applications, a key technology is the voltage-sensitive fluorescent protein, the development of which has seen recent progress [74–78]. This technology can give us a way to image cell-specific signals from unstained specimens. This emerging optogenetic tool can also be used with wide-field single-photon measurements, which share the same technical basis with VSD imaging. This method will be also useful for visualizing single-cell events among a large population of cells. That has been achieved with intracellular perfusion of the VSD [27, 79–81].

The progress in two-photon and SHG non-linear imaging also assures us that voltage imaging [82, 83] will eventually provide measurements of the nervous system over the whole range of scales, from the single dendritic spine to the entire brain.

Acknowledgments: We thank Dr. Michinori Ichikawa of BrainVision Inc. for teaching us information of the cameras and the fundamentals of the optical recordings.

References and Notes

1. D. K. Hill and R. D. Keynes, Opacity changes in stimulated nerve. *J. Physiol. (Lond)* 108, 278 (**1949**).
2. L. B. Cohen, R. D. Keynes, and B. Hille, Light scattering and birefringence changes during nerve activity. *Nature* 218, 438 (**1968**).
3. I. Tasaki, A. Watanabe, R. Sandlin, and L. Carnay, Changes in fluorescence tubidity and birefringence associated with nerve excitation, *Proc Natl Acad Sci USA* (**1968**), Vol. 61, pp. 883–888.
4. B. M. Salzberg, H. V. Davila, and L. B. Cohen, Optical recording of impulses in individual neurones of an invertebrate central nervous system. *Nature* 246, 508 (**1973**).
5. A. Grinvald, W. N. Ross, and I. Farber, Simultaneous optical measurements of electrical activity from multiple sites on processes of cultured neurons, *Proc. Natl. Acad. Sci. USA* (**1981**), Vol. 78, pp. 3245–3249.

6. D. M. Senseman, H. Shimizu, I. S. Horwitz, and B. M. Salzberg, Multiple-site optical recording of membrane potential from a salivary gland. Interaction of synaptic and electrotonic excitation. *J. Gen. Physiol.* 81, 887 **(1983)**.
7. L. B. Cohen and S. Lesher, Optical monitoring of membrane potential: methods of multisite optical measurement, Optical Methods in Cell Physiology, edited by P. DeWeer and B. M. Salzberg, Wiley, New York **(1986)**, Vol. 40, pp. 71–99.
8. L. B. Cohen and B. M. Salzberg, Optical measurement of membrane potential. *Rev. Physiol. Biochem. Pharmacol.* 83, 35 **(1978)**.
9. L. B. Cohen, B. M. Salzberg, and A. Grinvald, Optical methods for monitoring neuron activity. *Annu. Rev. Neurosci.* 1, 171 **(1978)**.
10. A. Grinvald, R. D. Frostig, E. Lieke, and R. Hildesheim, Optical imaging of neuronal activity. *Physiol. Rev.* 68, 1285 **(1988)**.
11. A. Grinvald and R. Hildesheim, VSDI: A new era in functional imaging of cortical dynamics. *Nat. Rev. Neurosci.* 5, 874 **(2004)**, [Doi:10.1038/nrn1536].
12. D. S. Peterka, H. Takahashi, and R. Yuste, Imaging voltage in neurons. *Neuron* 69, 9 **(2011)**, [Doi:10.1016/j.neuron.2010.12.010].
13. R. Homma, B. J. Baker, L. Jin, O. Garaschuk, A. Konnerth, L. B. Cohen, and D. Zecevic, Wide-field and two-photon imaging of brain activity with voltage- and calcium-sensitive dyes. *Philos. Trans. R Soc. Lond, B, Biol. Sci.* 364, 2453 **(2009)**, [Doi:10.1098/rstb.2009.0084].
14. M. Z. L. Kee, J. P. Wuskell, L. M. Loew, G. J. Augustine, and Y. Sekino, Imaging activity of neuronal populations with new long-wavelength voltage-sensitive dyes. *Brain Cell Biology* 36, 157 **(2008)**, [Doi:10.1007/s11068-009-9039-x].
15. Y. Momose-Sato, K. Sato, Y. Arai, I. Yazawa, H. Mochida, and K. Kamino, Evaluation of voltage-sensitive dyes for long-term recording of neural activity in the hippocampus *J. Membr. Biol.* 172, 145 **(1999)**.
16. Y. Momose-Sato, K. Sato, T. Sakai, A. Hirota, K. Matsutani, and K. Kamino, Evaluation of optimal voltage-sensitive dyes for optical monitoring of embryonic neural activity. *J. Membr. Biol.* 144, 167 **(1995)**.
17. E. H. Ratzlaff and A. Grinvald, A tandem-lens epifluorescence macroscope: Hundred-fold brightness advantage for wide-field imaging. *J. Neurosci. Methods* 36, 127 **(1991)**.
18. T. Tominaga, Y. Tominaga, H. Yamada, G. Matsumoto, and M. Ichikawa, Quantification of optical signals with electrophysiological signals in neural activities of Di-4-ANEPPS stained rat hippocampal slices. *J. Neurosci. Methods* 102, 11 **(2000)**.
19. A. Grinvald, L. B. Cohen, S. Lesher, and M. B. Boyle, Simultaneous optical monitoring of activity of many neurons in invertebrate ganglia using a 124-element photodiode array. *J. Neurophysiol.* 45, 829 **(1981)**.
20. T. Iijima, G. Matsumoto, and Y. Kidokoro, Synaptic activation of rat adrenal medulla examined with a large photodiode array in combination with a voltage-sensitive dye. *Neuroreport* 51, 211 **(1992)**.
21. A. Hirota, K. Sato, Y. Momose-Sato, T. Sakai, and K. Kamino, A new simultaneous 1020-site optical recording system for monitoring neural activity using voltage-sensitive dyes. *J. Neurosci. Methods* 56, 187 **(1995)**.
22. I. Takashima, M. Ichikawa, and T. Iijima, High-speed CCD imaging system for monitoring neural activity *in vivo* and *in vitro*, using a voltage-sensitive dye. *J. Neurosci. Methods* 91, 147 **(1999)**.
23. M. Ichikawa, T. Iijima, and G. Matsumoto, Real-Time optical recording of neuronal activities in the Brain, Brain Mechanisms of Perception and Memory, edited by T. Ono, L. R. Squire, M. E. Raichle, D. I. Perett, and M. Fukuda, Oxford UP, New York **(1993)**, pp. 638–648.
24. M. Nishimura, H. Shirasawa, and W.-J. Song, A light-emitting diode light source for imaging of neural activities with voltage-sensitive dyes. *Neurosci. Res.* 54, 230 **(2006)**, [Doi:10.1016/j.neures.2005.12.002].
25. L. M. Loew, L. B. Cohen, B. M. Salzberg, A. L. Obaid, and F. Bezanilla, Charge-shift probes of membrane potential. Characterization of aminostyrylpyridinium dyes on the squid giant axon. *Biophys. J.* 47, 71 **(1985)**, [Doi:10.1016/S0006-3495(85)83878-9].
26. L. M. Loew, L. B. Cohen, J. Dix, E. N. Fluhler, V. Montana, G. Salama, and J. Y. Wu, A naphthyl analog of the aminostyryl pyridinium class of potentiometric membrane dyes shows consistent sensitivity in a variety of tissue, cell, and model membrane preparations. *J. Membr. Biol.* 130, 1 **(1992)**.
27. S. Antic and D. Zecevic, Optical signals from neurons with internally applied voltage-sensitive dyes. *J. Neurosci.* 15, 1392 **(1995)**.
28. D. Shoham, D. E. Glaser, A. Arieli, T. Kenet, C. Wijnbergen, Y. Toledo, R. Hildesheim, and A. Grinvald, Imaging cortical dynamics at high spatial and temporal resolution with novel blue voltage-sensitive dyes. *Neuron* 24, 791 **(1999)**.
29. G. Carriero, L. Uva, V. Gnatkovsky, and M. de Curtis, Distribution of the olfactory fiber input into the olfactory tubercle of the *in vitro* isolated guinea pig brain. *J. Neurophysiol.* 101, 1613 **(2009)**, [Doi:10.1152/jn.90792.2008].
30. P. Y. Chang and M. B. Jackson, Heterogeneous spatial patterns of long-term potentiation in rat hippocampal slices. *J. Physiol. (Lond)* 576, 427 **(2006)**, [Doi:10.1113/jphysiol.2006.112128].
31. R. Kajiwara, T. Tominaga, and I. Takashima, Olfactory information converges in the amygdaloid cortex via the piriform and entorhinal cortices: Observations in the guinea pig isolated whole-brain preparation. *Eur. J. Neurosci.* 25, 3648 **(2007)**, [Doi:10.1111/j.1460-9568.2007.05610.x].
32. B. Renshaw, A. Forbes, and B. Morison, Activity of isocortex and hippocampus: Electrical studies with micro-electrodes. *J. Neurophysiol.* **(1940)**.
33. P. Andersen, T. V. P. Bliss, T. Lomo, L. I. Olsen, and K. K. Skrede, Lamellar organization of hippocampal excitatory pathways. *Acta Physiol. Scand* 76, 4A **(1969)**.
34. A. Grinvald, A. Manker, and M. Segal, Visualization of the spread of electrical activity in rat hippocampal slices by voltage-sensitive optical probes. *J. Physiol. (Lond)* 333, 269 **(1982)**.
35. M. E. Barish, M. Ichikawa, T. Tominaga, G. Matsumoto, and T. Iijima, Enhanced fast synaptic transmission and a delayed depolarization induced by transient potassium current blockade in rat hippocampal slice as studied by optical recording. *J. Neurosci.* 16, 5672 **(1996)**.
36. Y. Sekino, K. Obata, M. Tanifuji, M. Mizuno, and J. Murayama, Delayed signal propagation via CA2 in rat hippocampal slices revealed by optical recording. *J. Neurophysiol.* 78, 1662 **(1997)**.
37. Y. Nakagami, H. Saito, and N. Matsuki, Optical recording of trisynaptic pathway in rat hippocampal slices with a voltage-sensitive dye. *Neuroreport United States* 81, 1 **(1997)**.
38. S. Kojima, T. Nakamura, T. Nidaira, K. Nakamura, N. Ooashi, E. Ito, K. Watase, K. Tanaka, K. Wada et al., Optical detection of synaptically induced glutamate transport in hippocampal slices. *J. Neurosci.* 19, 2580 **(1999)**.
39. T. Tominaga, Y. Tominaga, and M. Ichikawa, Simultaneous multisite recordings of neural activity with an inline multi-electrode array and optical measurement in rat hippocampal slices. *Pflugers Arch.* 443, 317 **(2001)**, [Doi:10.1007/s004240100707].
40. K. Tanemura, M. Murayama, T. Akagi, T. Hashikawa, T. Tominaga, M. Ichikawa, H. Yamaguchi, and A. Takashima, Neurodegeneration with tau accumulation in a transgenic mouse expressing V337M human tau. *J. Neurosci.* 22, 133 **(2002)**.
41. T. Tominaga, Y. Tominaga, and M. Ichikawa, Optical imaging of long-lasting depolarization on burst stimulation in area CA1 of rat hippocampal slices. *J. Neurophysiol.* 88, 1523 **(2002)**.
42. E. Mann, T. Tominaga, and M. Ichikawa, Cholinergic modulation of the spatiotemporal pattern of hippocampal activity *in vitro*. *Neuropharmacology* **(2005)**.
43. E. O. Mann, J. M. Suckling, N. Hajos, S. A. Greenfield, and O. Paulsen, Perisomatic feedback inhibition underlies cholinergically

induced fast network oscillations in the rat hippocampus *in vitro*. *Neuron* 45, 105 (**2005**), [Doi:10.1016/j.neuron.2004.12.016].
44. S. Nakauchi, R. J. Brennan, J. Boulter, and K. Sumikawa, Nicotine gates long-term potentiation in the hippocampal CA1 region via the activation of alpha2* nicotinic ACh receptors. *Eur. J. Neurosci.* 25, 2666 (**2007**), [Doi:10.1111/j.1460-9568.2007.05513.x].
45. M. Nakamura, Y. Sekino, and T. Manabe, GABAergic interneurons facilitate mossy fiber excitability in the developing hippocampus. *J. Neurosci.* 27, 1365 (**2007**), [Doi:10.1523/JNEUROSCI.4672-06.2007].
46. Y. Tominaga, M. Ichikawa, and T. Tominaga, Membrane potential response profiles of CA1 pyramidal cells probed with voltage-sensitive dye optical imaging in rat hippocampal slices reveal the impact of GABA(A)-mediated feed-forward inhibition in signal propagation. *Neurosci. Res.* 64, 152 (**2009**), [Doi:10.1016/j.neures.2009.02.007].
47. T. Tominaga and Y. Tominaga, GABAA receptor-mediated modulation of neuronal activity propagation upon tetanic stimulation in rat hippocampal slices. *Pflugers Arch.* 460, 875 (**2010**), [Doi:10.1007/s00424-010-0870-9].
48. H. Mochida, K. Sato, S. Sasaki, I. Yazawa, K. Kamino, and Y. Momose-Sato, Effects of anisomycin on LTP in the hippocampal CA1: Long-term analysis using optical recording. *Neuroreport* 12, 987 (**2001**).
49. L. Chen and M. Sokabe, Presynaptic modulation of synaptic transmission by pregnenolone sulfate as studied by optical recordings. *J. Neurophysiol.* 94, 4131 (**2005**), [Doi:10.1152/jn.00755.2004].
50. T. Aihara, Y. Kobayashi, and M. Tsukada, Spatiotemporal visualization of long-term potentiation and depression in the hippocampal CA1 area. *Hippocampus* 15, 68 (**2005**), [Doi:10.1002/hipo.20031].
51. L. Chen, K. Yamada, T. Nabeshima, and M. Sokabe, Alpha7 Nicotinic acetylcholine receptor as a target to rescue deficit in hippocampal LTP induction in beta-amyloid infused rats. *Neuropharmacology* 50, 254 (**2006**), [Doi:10.1016/j.neuropharm.2005.09.018].
52. T. Aihara, Y. Abiru, Y. Yamazaki, H. Watanabe, Y. Fukushima, and M. Tsukada, The relation between spike-timing dependent plasticity and Ca(2+) dynamics in the hippocampal CA1 network. *Neuroreport* 145, 80 (**2007**).
53. A. Kasuga, R. Enoki, Y. Hashimoto, H. Akiyama, Y. Kawamura, M. Inoue, Y. Kudo, and H. Miyakawa, Optical detection of dendritic spike initiation in hippocampal CA1 pyramidal neurons. *Neuroreport* 118, 899 (**2003**).
54. R. Enoki, M. Inoue, Y. Hashimoto, Y. Kudo, and H. Miyakawa, GABAergic control of synaptic summation in hippocampal CA1 pyramidal neurons. *Hippocampus* 11, 683 (**2001**), [Doi:10.1002/hipo.1083].
55. R. Enoki, M. Namiki, Y. Kudo, and H. Miyakawa, Optical monitoring of synaptic summation along the dendrites of CA1 pyramidal neurons. *Neuroreport* 113, 1003 (**2002**).
56. M. Inoue, Y. Hashimoto, Y. Kudo, and H. Miyakawa, Dendritic attenuation of synaptic potentials in the CA1 region of rat hippocampal slices detected with an optical method. *Eur. J. Neurosci.* 13, 1711 (**2001**).
57. M. Tanifuji, T. Sugiyama, and K. Murase, Horizontal propagation of excitation in rat visual cortical slices revealed by optical imaging. *Science United States* 266, 1057 (**1994**).
58. T. R. Barkat, D. B. Polley, and T. K. Hensch, A critical period for auditory thalamocortical connectivity. *Nat. Neurosci.* 14, 1189 (**2011**), [doi:10.1038/nn.2882].
59. T. Iijima, M. P. Witter, M. Ichikawa, T. Tominaga, R. Kajiwara, and G. Matsumoto, Entorhinal-hippocampal interactions revealed by real-time imaging. *Science* 272, 1176 (**1996**).
60. N. Koganezawa, A. Taguchi, T. Tominaga, S. Ohara, K.-I. Tsutsui, M. P. Witter, and T. Iijima, Significance of the deep layers of entorhinal cortex for transfer of both perirhinal and amygdala inputs to the hippocampus. *Neurosci. Res.* 61, 172 (**2008**), [Doi:10.1016/j.neures.2008.02.007].
61. N. Cappaert, F. Lopes da Silva, and W. Wadman, Spatio-temporal dynamics of theta oscillations in hippocampal-entorhinal slices. *Hippocampus* 19, 1065 (**2009**), [Doi:10.1002/hipo.20570].
62. J. Suh, A. J. Rivest, T. Nakashiba, T. Tominaga, and S. Tonegawa, Entorhinal cortex layer III input to the hippocampus is crucial for temporal association memory. *Science* 334, 1415 (**2011**), [Doi:10.1126/science.1210125].
63. R. Kajiwara, I. Takashima, Y. Mimura, M. P. Witter, and T. Iijima, Amygdala input promotes spread of excitatory neural activity from perirhinal cortex to the entorhinal-hippocampal circuit. *J. Neurophysiol.* 89, 2176 (**2003**), [Doi:10.1152/jn.01033.2002].
64. M. De Curtis, I. Takashima, and T. Iijima, Optical recording of cortical activity after *in vitro* perfusion of cerebral arteries with a voltage-sensitive dye. *Brain Res.* 837, 314 (**1999**).
65. H. Onimaru, A. Kanamaru, and I. Homma, Optical imaging of respiratory burst activity in newborn rat medullary block preparations. *Neurosci. Res.* 25, 183 (**1996**).
66. H. Onimaru and I. Homma, A novel functional neuron group for respiratory rhythm generation in the ventral medulla. *J. Neurosci.* 23, 1478 (**2003**).
67. H. Onimaru and I. Homma, Spontaneous oscillatory burst activity in the piriform-amygdala region and its relation to *in vitro* respiratory activity in newborn rats. *Neuroreport* 144, 387 (**2007**), [Doi:10.1016/j.neuroscience.2006.09.033].
68. A. Arata and M. Ito, Purkinje cell functions in the *in vitro* cerebellum isolated from neonatal rats in a block with the pons and medulla. *Neurosci. Res.* 50, 361 (**2004**), [Doi:10.1016/j.neures.2004.08.011].
69. A. Arata and M. Ito, Synaptic transmission and long-term depression in Purkinje cells in an *in vitro* block preparation of the cerebellum isolated from neonatal rats. *Prog. Brain Res.* 148, 111 (**2005**), [Doi:10.1016/S0079-6123(04)48010-8].
70. K. Sato, H. Mochida, I. Yazawa, S. Sasaki, and Y. Momose-Sato, Optical approaches to functional organization of glossopharyngeal and vagal motor nuclei in the embryonic chick hindbrain. *J. Neurophysiol.* 88, 383 (**2002**).
71. Y. Momose-Sato, H. Mochida, S. Sasaki, and K. Sato, Depolarization waves in the embryonic CNS triggered by multiple sensory inputs and spontaneous activity: Optical imaging with a voltage-sensitive dye. *Neuroreport* 116, 407 (**2003**).
72. P. J. Uhlhaas and W. Singer, Neuronal dynamics and neuropsychiatric disorders: Toward a translational paradigm for dysfunctional large-scale networks. *Neuron* 75, 963 (**2012**), [Doi:10.1016/j.neuron.2012.09.004].
73. T. Tominaga and Y. Tominaga, A new non-scanning confocal microscopy module for functional voltage-sensitive dye and Ca^{2+} imaging of neuronal circuit activity. *J. Neurophysiol.* (**2013**), [Doi:10.1152/jn.00856.2012].
74. B. J. Baker, H. Mutoh, D. Dimitrov, W. Akemann, A. Perron, Y. Iwamoto, L. Jin, L. B. Cohen, E. Y. Isacoff et al., Genetically encoded fluorescent sensors of membrane potential. *Brain Cell Biology* 36, 53 (**2008**), [Doi:10.1007/s11068-008-9026-7].
75. T. Knöpfel, Expanding the toolbox for remote control of neuronal circuits. *Nat Methods* 5, 293 (**2008**), [Doi:10.1038/nmeth0408-293].
76. L. Jin, Z. Han, J. Platisa, J. R. A. Wooltorton, L. B. Cohen, and V. A. Pieribone, Single action potentials and subthreshold electrical events imaged in neurons with a fluorescent protein voltage probe. *Neuron* 75, 779 (**2012**), [Doi:10.1016/j.neuron.2012.06.040].
77. T. Knöpfel, Genetically encoded optical indicators for the analysis of neuronal circuits. *Nat. Rev. Neurosci.* 13, 687 (**2012**), [Doi:10.1038/nrn3293].
78. W. Akemann, H. Mutoh, A. Perron, J. Rossier, and T. Knöpfel, Imaging brain electric signals with genetically targeted voltage-sensitive fluorescent proteins. *Nat. Methods* 7, 643 (**2010**), [Doi:10.1038/nmeth.1479].
79. S. Antic, G. Major, and D. Zecevic, Fast optical recordings of membrane potential changes from dendrites of pyramidal neurons. *J. Neurophysiol.* 82, 1615 (**1999**).

80. D. Zecevic, Multiple spike-initiation zones in single neurons revealed by voltage-sensitive dyes. *Nature* 381, 322 (**1996**), [Doi:10.1038/381322a0].

81. D. Zecevic and S. Antic, Fast optical measurement of membrane potential changes at multiple sites on an individual nerve cell. *Histochem. J.* 30, 197 (**1998**).

82. D. A. Dombeck, M. Blanchard-Desce, and W. W. Webb, Optical recording of action potentials with second-harmonic generation microscopy. *J. Neurosci.* 24, 999 (**2004**). [Doi:10.1523/JNEUROSCI.4840-03.2004].

83. M. Nuriya, J. Jiang, B. Nemet, K. B. Eisenthal, and R. Yuste, Imaging membrane potential in dendritic spines, *Proc. Natl. Acad. Sci. USA* 103, 786 (**2006**), Doi:10.1073/pnas.0510092103.

A new nonscanning confocal microscopy module for functional voltage-sensitive dye and Ca^{2+} imaging of neuronal circuit activity

Takashi Tominaga and Yoko Tominaga

J Neurophysiol 110:553-561, 2013. First published 24 April 2013;
doi: 10.1152/jn.00856.2012

Journal of Neurophysiology publishes original articles on the function of the nervous system. It is published 24 times a year (twice monthly) by the American Physiological Society, 9650 Rockville Pike, Bethesda MD 20814-3991. ESSN: 1522-1598. Visit our website at http://www.the-aps.org/.

J Neurophysiol 110: 553–561, 2013.
First published April 24, 2013; doi:10.1152/jn.00856.2012.

A new nonscanning confocal microscopy module for functional voltage-sensitive dye and Ca^{2+} imaging of neuronal circuit activity

Takashi Tominaga and Yoko Tominaga

Laboratory for Neural Circuit Systems, Institute of Neuroscience, Tokushima Bunri University, Shido, Sanuki, Kagawa, Japan

Submitted 24 September 2012; accepted in final form 22 April 2013

Tominaga T, Tominaga Y. A new nonscanning confocal microscopy module for functional voltage-sensitive dye and Ca^{2+} imaging of neuronal circuit activity. *J Neurophysiol* 110: 553–561, 2013. First published April 24, 2013; doi:10.1152/jn.00856.2012.—Recent advances in fluorescent confocal microscopy and voltage-sensitive and Ca^{2+} dyes have vastly improved our ability to image neuronal circuits. However, existing confocal systems are not fast enough or too noisy for many live-cell functional imaging studies. Here, we describe and demonstrate the function of a novel, nonscanning confocal microscopy module. The optics, which are designed to fit the standard camera port of the Olympus BX51WI epifluorescent microscope, achieve a high signal-to-noise ratio (SNR) at high temporal resolution, making this configuration ideal for functional imaging of neuronal activities such as the voltage-sensitive dye (VSD) imaging. The optics employ fixed 100- × 100-pinhole arrays at the back focal plane (optical conjugation plane), above the tube lens of a usual upright microscope. The excitation light travels through these pinholes, and the fluorescence signal, emitted from subject, passes through corresponding pinholes before exciting the photodiodes of the imager: a 100- × 100-pixel metal-oxide semiconductor (MOS)-type pixel imager with each pixel corresponding to a single 100- × 100-μm photodiode. This design eliminated the need for a scanning device; therefore, acquisition rate of the imager (maximum rate of 10 kHz) is the only factor limiting acquisition speed. We tested the application of the system for VSD and Ca^{2+} imaging of evoked neuronal responses on electrical stimuli in rat hippocampal slices. The results indicate that, at least for these applications, the new microscope maintains a high SNR at image acquisition rates of ≤0.3 ms per frame.

confocal microscopy; hippocampal slice; voltage-sensitive dye; optical imaging; Ca^{2+} imaging

CONFOCAL MICROSCOPY (Amos and White 2003; Pawley 2006) is of increasing importance in functional imaging of neuronal circuit (Bullen et al. 1997; Ikegaya et al. 2004; Ohki et al. 2005). However, existing confocal systems are not fast enough for many high-speed imaging applications because the temporal resolution is limited (Saggau 2006). The aim of our study was to develop confocal optics that can be used for functional imaging that requires fast image acquisition rates such as voltage-sensitive dye (VSD) imaging (Cohen et al. 1978; Grinvald and Hildesheim 2004; Peterka et al. 2011; Peterlin et al. 2000).

VSD imaging of rapid changes of membrane potential, such as action potentials, requires a frame rate of ≥1 kHz (Grinvald et al. 1982; Ichikawa et al. 1993; Tominaga et al. 2000, 2009; Vranesic et al. 1994). Because VSD signals are often as small as 10^{-4} of baseline fluorescence, large numbers of photons must be sampled during short time intervals to achieve a sufficient signal-to-noise ratio (SNR). This is because photon shot noise expressed as fraction of baseline fluorescence decreases with 1 per square root of the number of photons (Knöpfel et al. 2006). This is difficult to achieve with a conventional confocal microscope because their frame rate is limited and they are not sampling large numbers of photons.

Most confocal microscopes, including laser-scanning, Nipkow disk, and swept-field confocal microscopy, rely on some type of scanning mechanism to acquire an image, thus limiting image acquisition speed (Kino 1995). The optical system that we have developed eliminates the need for a scanning mechanism, using, instead, fixed arrays of pinholes that correspond to a photodiode array on the imager. Our complementary metal-oxide semiconductor (CMOS) imaging system (Tominaga et al. 2005; same as MiCAM Ultima BrainVision) is composed of only a 100- × 100-pixel photodiode array but has a very high frame rate (10 kHz) at high SNR (70 dB). Each photodiode has a maximum surface area of 10,000 μm^2. This imager enabled us to use a nonscanning pinhole array with each pinhole corresponding to a unique pixel of the imager.

The confocal microscopy module was designed to fit the standard camera port of an epifluorescent microscope (BX51WI; Olympus). We tested the microscope by imaging a hippocampal slice preparation of rat by bulk VSD and Ca^{2+} indicator staining. The results demonstrate that the module can achieve fast acquisition in a confocal configuration without introducing noise associated with traditional scanning confocal microscopes.

MATERIALS AND METHODS

Optical configuration. A schematic diagram of the nonscanning confocal microscope is shown in Fig. 1. The confocal microscope consists of an infinity correction epifluorescent microscope (BX51WI) and our confocal microscopy module. Light from a xenon arc lamp (75-W Xe-lamp; U-LH75EAPO; Olympus) was introduced via a large core fiber optic cable [core diameter = 3 mm, numerical aperture (NA) = 0.48] and passed through an excitation filter of a mirror unit (compatible with Olympus microscope mirror unit, U-MF/XL). An electrical shutter (Copal 0 Shutter) was placed in the fiber optics condenser unit. The excitation light was reflected through a secondary objective lens onto a pinhole array plate (Fig. 1*B*) positioned in the intermediate image plane. The excitation light passing through each pinhole (P and P′) was focused onto corresponding focus points (O and O′) on the sample. Fluorescent light, emitted from each focal point on the sample, was then projected onto the same pinhole array by the objective lens (×20 NA 1.0; Olympus) and tube lens (f = 180 mm) of the epifluorescent microscope. So that the focal plane of the sample and the pinhole array plate were in optical phase conjugation, the fluorescence passing through each pinhole was collected by a

Address for reprint requests and other correspondence: T. Tominaga, Laboratory for Neural Circuit Systems, Institute of Neuroscience, Tokushima Bunri Univ., 1314-1 Shido, Sanuki, Kagawa 769-2193, Japan (e-mail: tominagat@kph.bunri-u.ac.jp).